University of Warwick institutional repository

Authors:	Sergey Nazarenko and Brenda Quinn
Article title:	Triple Cascade Behavior in Quasigeostrophic and Drift Turbulence and Generation of Zonal Jets
Year of publication:	2009
Link to published version:	http://dx.doi.org/ 10.1103/PhysRevLett.103.118501
Publisher statement:	None

a

Triple cascade behaviour in QG and drift turbulence and generation of zonal jets

Sergey Nazarenko, Brenda Quinn

Abstract We study quasi-geostrophic turbulence and plasma drift turbulence within the Charney-Hasegawa-Mima (CHM) model. We focus, theoretically and using numerical simulations, on conservation of *zonostrophy* and on its role in the formation of the zonal jets. The zonostrophy invariant was first predicted in [1, 2] in two special cases – large-scale turbulence and anisotropic turbulence. Papers [1, 2] also predicted that the three invariants, energy, enstrophy and zonostrophy, will cascade anisotropically into non-intersecting sectors in the k-space, so that the energy cascade is "pushed" into the large-scale zonal scales. In the present paper, we consider the scales much less than the Rossby deformation radius and generalise the Fjørtoft argument of [1, 2] to find the directions of the three cascades in this case. For the first time, we demonstrate numerically that zonostrophy is well conserved by the CHM model, and that the energy, enstrophy and zonostrophy cascade as prescribed by the Fjørtoft argument if the nonlinearity is sufficiently weak. Moreover, numerically we observe that zonostrophy is conserved surprisingly well at late times and the triple-cascade picture is rather accurate even if the initial nonlinearity is strong.

1 Introduction and the model

Zonal jets are prominent features in geophysical fluids, e.g. atmospheres of Jupiter and Saturn [4, 5, 6] and the earths' atmosphere [10, 3] and oceans [3, 6, 7]. Zonal jets have also been observed in fusion plasmas [15]. Zonal jets are important be-

———————————————

Sergey Nazarenko

Mathematics Institute, University of Warwick, Gibbet Hill Road, Coventry CV4 7AL, UK, e-mail: S.V.Nazarenko@.warwick.ac.uk

Brenda Quinn

Mathematics Institute, University of Warwick, Gibbet Hill Road, Coventry CV4 7AL, UK e-mail: B.E.Quinn@warwick.ac.uk

cause they can suppress the small-scale turbulence and block the transport in both geophysical settings [11] and in plasmas [12, 14, 15].

Two main zonal jet generation mechanisms considered in the literature are the modulational instability [16, 8, 17, 9, 18, 19, 20, 21] and the anisotropic inverse cascade [22, 26, 23, 12]. The inverse cascade mechanism brings the energy from initial small-scale turbulence to the large-scale zonal flows in a step-by-step (local in the scale space) transfer mechanism similar to the inverse cascade in 2D Navier-Stokes turbulence [24, 25]. On the other hand, the modulational instability brings energy to the large zonal scales directly, skipping the intermediate scales. It appears to be more relevant if the small-scale turbulence has a narrow initial spectrum, whereas the cascade picture is more accurate when the initial spectrum is broad. We will report on our recent analytical and numerical studies of the modulational instability elsewhere [21], whereas the present paper will focus on the turbulent cascades.

The mechanism for an inverse cascade in geophysical quasi-geostrophic (QG) turbulence and in plasma drift turbulence is quite similar to the one of the 2D Navier-Stokes turbulence [24, 25], but the presence of the beta-effect (non-uniform rotation of geophysical fluids or plasma inhomogeneity) makes this cascade anisotropic leading to condensation into large-scale zonal flows rather than round vortices [22, 26, 23].

In this paper we will follow the approach put forward in papers [1, 2] which is most relevant (and asymptotically rigorous) when the QG/drift turbulence is weak. In this case the turbulence is dominated by waves which are involved in triad interactions. These three-wave interactions are shown to conserve an additional positive quadratic invariant. This invariant and the other two quadratic invariants, the energy and the potential enstrophy, are involved in a triple cascade process, which can be described via an argument similar to the standard Fjørtoft argument originally developed for the 2D Navier-Stokes turbulence [24]. It was found that each of the invariants is forced by the other two to cascade into its own anisotropic sector of scales and, in particular, the energy is forced to cascade to long zonal scales. Considering its important role in the zonation process, hereafter we will label the extra invariant as *zonostrophy*.

On the other hand, work [1, 2] was limited to considering either very large scales (longer than the Rossby deformation radius or the Larmor radius) or to the scales which are already anisotropic and are close to zonal. Besides, the conservation of the extra invariant is based on the weakness of nonlinearity and on the randomness of phases (conditions of validity of the wave kinetic equation), which, even when present initially, can break down later on during the zonation process. Thus, numerical checks of robustness of the zonostrophy conservation were needed, and they have not been done until the work reported in the present paper.

Soon after papers [1, 2], the zonostrophy invariant was generalized to the whole of the *k*-space in [27]. This was a significant achievement because the extra invariant of such a kind appeared to be unique for Rossby/drift systems and is not observed in any other known nonlinear wave model [28]. Besides, its conservation has revealed interesting geometrical properties of the wave dispersion relation [28]. Unfortunately, the general expression for zonostrophy appeared to have a form for

which the Fjørtoft argument cannot be used (not scale invariant, not sign-definite). However, an alternative zonation argument was put forward in [29].

In the present paper we will focus on the special case when the scales are much smaller than the deformation (Larmor) radius, which is the most important and frequently considered limit (at least in the GFD context). Taking the respective limit in the general zonostrophy expression obtained in [27], we obtain the zonostrophy expression for such small-scale turbulence and show that it is positive and scale invariant. The latter observation is extremely important because it means that we can once again apply the generalized Fjørtoft argument developed in [1, 2], which is done in the present paper. Note that the Fjørtoft argument of [1, 2] is somewhat preferential over the argument presented in [29] because it predicts not only zonation but also the anisotropic k-space flow paths of the three invariants during the zonation process.

Having obtained these analytical predictions, we then proceed to direct numerical simulations (DNS) of the QG/drift turbulence to (i) test the conservation of the zonostrophy for different levels of initial nonlinearity, and (ii) test predictions of the generalized Fjørtoft argument by tracking in time the transfer path of the three invariants in the k-space. As a result, we confirm conservation of zonostrophy and its important role in directing the energy to the zonal jet scales.

2 Charney-Hasegawa-Mima model

The reason why geophysical quasi-geostrophic (QG) flows and plasma drift turbulence are often mentioned together (in particular when discussing the zonal jet formation) is that some basic linear and nonlinear properties in these two systems can be described by the same PDE, the Charney-Hasegawa-Mima (CHM) equation [30, 31]:

$$\partial_t \Delta \psi + \beta \partial_x \psi + (\partial_x \psi)\partial_y \Delta \psi - (\partial_y \psi)\partial_x \Delta \psi = 0, \qquad (1)$$

where ψ is the streamfunction, β is a constant proportional to the gradient of the horizontal rotation frequency or of the plasma density in the GFD and plasma contexts respectively. In the GFD context, the x-axis is in the west-east and the y-axis is along the south-north directions respectively. In plasmas, the y-axis is along the plasma density gradient and the x-axis, of course, is transverse to this direction. Here, we consider only small-scale turbulence with scales much smaller than the Rossby deformation radius in GFD and the ion Larmor radius in plasma contexts (this has already been taken into account in the CHM model, (1)).

Let us put our system in a periodic square box with side length L and introduce the Fourier transform of the streamfunction,

$$\psi_{\mathbf{k}} = \frac{1}{L^2} \int \psi(\mathbf{x}) e^{-i\mathbf{k} \cdot \mathbf{x}} d\mathbf{x},$$

where $\mathbf{k} = (k_x, k_y)$ is a wavevector in the 2D plane. In k-space the CHM equation (1) becomes:

$$\partial_t \hat{\psi}_{\mathbf{k}} = i\,\omega_{\mathbf{k}}\,\hat{\psi}_{\mathbf{k}} + \frac{1}{2} \sum_{\mathbf{k}_1+\mathbf{k}_2=\mathbf{k}} T(\mathbf{k},\mathbf{k}_1,\mathbf{k}_2)\,\hat{\psi}_{\mathbf{k}_1}\,\hat{\psi}_{\mathbf{k}_2}\,, \tag{2}$$

where

$$\omega_{\mathbf{k}} = -\frac{\beta k_x}{k^2} \tag{3}$$

is the dispersion relation for the frequency of linear waves (Rossby or drift waves in the GFD and plasma contexts respectively), $k = |\mathbf{k}|$, and

$$T(\mathbf{k},\mathbf{k}_1,\mathbf{k}_2) = -\frac{(\mathbf{k}_1 \times \mathbf{k}_2)_z\,(k_1^2 - k_2^2)}{k^2} \tag{4}$$

is a nonlinear interaction coefficient.

3 Conservation of energy and enstrophy

It is well known that the CHM equation, (1) conserves the energy and the enstrophy which in physical space are defined respectively as

$$E = \frac{1}{2} \int (\nabla \psi)^2\, d\mathbf{x} \tag{5}$$

and

$$\Omega = \frac{1}{2} \int (\triangle \psi)^2\, d\mathbf{x}. \tag{6}$$

In Fourier space these conserved quantities can be expressed in terms of the wave action

$$n(\mathbf{k}) = \frac{k^4 |\hat{\psi}_k|^2}{2\beta k_x}.$$

We have

$$E = \int |\omega_{\mathbf{k}}| n_{\mathbf{k}}\, d\mathbf{k} \tag{7}$$

and

$$\Omega = \int k_x n_{\mathbf{k}}\, d\mathbf{k}. \tag{8}$$

4 Conservation of zonostrophy.

The energy and the enstrophy are *exact* invariants of the small-scale CHM model (1). *Zonostrophy* is an exact invariant of the *kinetic equation*:

$$\dot{n}_{\mathbf{k}} = \int |V_{12k}|^2 \delta(\mathbf{k}_1 + \mathbf{k}_2 - \mathbf{k})\delta(\omega(\mathbf{k}_1) + \omega(\mathbf{k}_2) - \omega(\mathbf{k})) \times$$
$$[n(\mathbf{k}_1)n(\mathbf{k}_2) - 2n(\mathbf{k})n(\mathbf{k}_1)\operatorname{sign} - n(\mathbf{k})n(\mathbf{k}_2)\operatorname{sign}(k_x k_{2x})] \, d\mathbf{k}_1 d\mathbf{k}_2,$$

where

$$V_{12k} = |k_x k_{1x} k_{2x}|^{1/2} \left(\frac{k_{1y}}{k_1^2} + \frac{k_{2y}}{k_2^2} - \frac{k_y}{k^2} \right).$$

Thus, it should be clear that the zonostrophy is only proven to be a conserved quantity under the same conditions for which the kinetic equation (9) is valid, namely *weak nonlinearity* and *random phases*. It is presently unknown if the zonostrophy conservation extends to a broader range of situations or not. Thus, the numerical tests of zonostrophy conservation are crucial, and this is one of the aims of the present work.

In terms of the wave action spectrum, zonostrophy Z can be written as

$$Z = \int \zeta_{\mathbf{k}} n_{\mathbf{k}} \, d\mathbf{k}, \tag{9}$$

where function $\zeta_{\mathbf{k}}$ is the density of zonostrophy in the k-space which satisfies the triad resonance condition

$$\zeta(\mathbf{k}) = \zeta(\mathbf{k}_1) + \zeta(\mathbf{k}_2) \tag{10}$$

for all wavevectors $\mathbf{k}, \mathbf{k}_1$ and $\mathbf{k}_2$ which lie on the resonant surface given by the solutions of the wavevector and frequency resonance conditions,

$$\mathbf{k} = \mathbf{k}_1 + \mathbf{k}_2 \tag{11}$$

and

$$\omega(\mathbf{k}) = \omega(\mathbf{k}_1) + \omega(\mathbf{k}_2). \tag{12}$$

Expressions for $\zeta_{\mathbf{k}}$ were first found in [1, 2] in the special cases of large-scale turbulence ($\rho k \ll 1$ where ρ is the Rossby deformation radius in GFD or ion Larmor radius in plasmas) and for anisotropic turbulence ($k_x \ll k_y$), after which a general expression was found for all $\mathbf{k}$'s in [27]. This expression is

$$\zeta(\mathbf{k}) = \arctan \frac{k_y + k_x\sqrt{3}}{\rho k^2} - \arctan \frac{k_y - k_x\sqrt{3}}{\rho k^2}. \tag{13}$$

This expression can change sign and it is not a scale-invariant function of the wavevector components, which means that one cannot use the generalized Fjørtoft argument of [1, 2] to find the cascade directions in such a general case.

To find zonostrophy in the special case of small-scale turbulence (which is considered in the present paper) we have to take the limit $\rho k \to \infty$ in the general expression (13). It turns out that naively taking limit leads to an already known integral, the energy and one has to go to further orders in the Taylor expansion of (13) until we reach an expression which is independent of E and Ω. Interestingly, such an independent invariant appears only in the fifth order, and the derivation details are

given in Appendix A. The result is

$$\tilde{\zeta} = -\lim_{\rho \to \infty} \frac{5\rho^5}{8\sqrt{3}}(\zeta - 2\sqrt{3}\omega/\beta\rho) = \frac{k_x^3}{k^{10}}(k_x^2 + 5k_y^2). \tag{14}$$

The integral (9) with the density (14) is an exact invariant of the kinetic equation (9) and thus it is an *approximate* invariant of the small-scale CHM equation (1). Later on we will examine numerically the precision with which this invariant is conserved.

Expression (14) for the new invariant in the small-scale limit, $\rho k \gg 1$, allows us to explicitly see that the invariant's density is strictly positive and scale-invariant, which is good news because once again one can use the generalized Fjørtoft argument of [1, 2] to find the cascade directions of the three invariants: the energy, the enstrophy and the zonostrophy.

5 Triple cascade behaviour.

5.1 Dual cascades in 2D Navier-Stokes turbulence.

Before we present the generalized Fjørtoft argument, we will remind the reader of the classical Fjørtoft argument leading to the prediction of the dual cascade behaviour in 2D Navier-Stokes turbulence [24]. This will be instructive because by now there exists several versions of such an argument and the one we use here is not necessarily the most familiar.
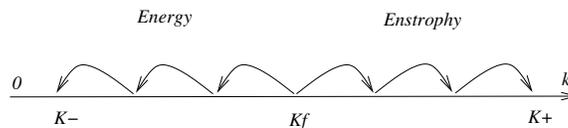
Fig. 1 Dual cascade behaviour in 2D Navier-Stokes turbulence.

Let us consider 2D turbulence described by the Navier-Stokes equations excited at some forcing scale $\sim k_0$ and dissipated at very large ($\sim k_- \ll k_0$) and at very small scales ($\sim k_+ \gg k_0$), see Fig. 1. The conservative ranges between the forcing scale and the dissipation scales, $k_- \ll k \ll k_0$ and $k_0 \ll k \ll k_+$ are called the inertial ranges. The two conserved quantities in this case, in the absence of forcing and dissipation, are the energy and the enstrophy which are given by the same expressions as for the small-scale CHM model, namely by (5) and (6) in the x-space and by (7) and (8) in the k-space. In the presence of forcing and dissipation in steady-state turbulence, the rate of production of the energy and the enstrophy by forcing must be exactly the same as the dissipation rates, ε and η respectively. Our task now is to determined where exactly E and Ω are dissipated, at $\sim k_-$ or at $\sim k_+$.

First, we note that the k-space densities of E and Ω differ by a factor of k^2, and therefore the energy dissipation rate ε is related to the enstrophy dissipation rate η as $\eta \sim k_0{}^2 \varepsilon$. Now, let us suppose *ad absurdum* that at $\sim k_+$ the energy is dissipated at a rate comparable to the rate of production at the forcing scales, i.e. $\sim \varepsilon$. But this would mean that the enstrophy would be dissipated at the rate $\sim k_+^2 \varepsilon$ which is impossible in steady state since this amount greatly exceeds the rate of the enstrophy production $\eta \sim\sim k_0{}^2 \varepsilon$. Thus we conclude that most of the energy must be dissipated at the scales $\sim k_-$, i.e. that the energy cascade is *inverse* (with respect to its direction in 3D turbulence).

Similarly, assuming *ad absurdum* that most of the enstrophy is dissipated at $\sim k_-$ would also lead to a conclusion that the amount of energy dissipated is much greater than the energy produced, which is impossible. Therefore, the enstrophy cascade is direct, i.e. it is dissipated at wavenumbers $\sim k_+$ which are greater than the forcing scale k_0.

5.2 Triple cascades in CHM turbulence.

From the Fjørtoft argument presented above, the reader should notice that the quantities that determine the cascade directions are the k-space densities of the invariants or, more precisely, the scaling of the ratios of these densities with k. It is also important that these k-space densities are positive (as is the case for E, Ω and Z in our situation, see (7), (8) and (14)) because otherwise a large positive and a large negative amount of the same invariant could be produced in different corners of the k-space, with the net result zero and the Fjørtoft argument would not work. Further, it is important that all of the invariants have the same scaling with respect to the turbulence intensity so that their ratios are functions of $\mathbf{k}$ and not of the turbulent intensity. This condition is satisfied, for both Navier-Stokes and in the CHM model since E, Ω and Z are linear in n_k, see (7), (8) and (14).

The ratio of the k-space densities of Ω and E is k^2 which allows us to conclude that Ω must go to $k \gg k_0$ and E must cascade to $k \ll k_0$. In other words, each of the invariants cascades to the scales where its density is dominant over the density of the other invariant. This argument is easily generalizable to the CHM model and the respective three invariants, E, Ω and Z. Now we have three invariants, and the cascade picture would necessarily be anisotropic (it is impossible to divide the 2D $\mathbf{k}$-space into three non-intersecting cascade regions in an isotropic way).

Let us suppose that turbulence is produced near $\mathbf{k}_0 = (k_{0x}, k_{0y})$ and it can be dissipated only in regions which are separated in scales from the forcing scale, i.e. either at $k \gg k_0$ (short scales), or at $k_x \ll k_{0x}$ (nearly zonal scales), or at $k_y \ll k_{0y}$ (nearly meridional scales), see Fig. (2). Then each of the invariants (e.g. E), must cascade to the scales where its density is dominant over the densities of the other two invariants (e.g. Ω and Z). The boundaries between the cascading ranges lie on the curves in the k-space where the ratios of the different invariant densities (taken pairwise) remain constant (equal to the respective initial values).

We note that because $k^2 \le k_x{}^2 + 5k_y{}^2 \le 5k^2$, and because because the Fjørtoft argument operates only with the strong inequalities ($\gg$ and $\ll$ rather than $>$ and $>$), we can replace the zonostrophy density (14) with a simpler expression,

$$\tilde{\zeta}_{\mathbf{k}} \sim \frac{k_x{}^3}{k^8}. \tag{15}$$

Thus we have for the boundaries between the different cascade sectors, see Fig. (2):

- *E/Ω boundary:* As for the 2D Navier-Stokes turbulence considered before, we have for this boundary separating the energy and the enstrophy cascades,

$$k^2 \sim k_0^2, \tag{16}$$

  (i.e. a circle in the 2D k-space, $k_x^2 + k_y^2 = k_0^2$.)

- *E/Z boundary:* Equating the ratio of the energy density $|\omega_k|$ to the zonostropy density $k_x{}^3/k^8$ to the initial value of this ratio, we get for the boundary separating the energy and the zonostrophy cascades,

$$k^3/k_x \sim k_0^3/k_{0x}. \tag{17}$$

- *Ω/Z boundary:* Equating the ratio of the enstrophy density k_x to the zonostropy density $k_x{}^3/k^8$ to the initial value of this ratio, we get for the boundary separating the enstrophy and the zonostrophy cascades,

$$k^4/k_x \sim k_0^4/k_{0x}. \tag{18}$$

The first of these expressions, (16), says that (like in 2D turbulence before) the energy must go to larger scales and the enstrophy must go to smaller scales.

The second expression, (17), says that the energy must go to the zonal scales, $k_y \gg k_x$. Moreover, this expression also poses a particular restriction on the path of the energy to the zonal scales, e.g. for $k_y \gg k_x$ it should zonate at least as fast as $k_y = \text{const } k_x^{1/3}$, see Fig. (2).

The last relation, (18), is also interesting. Because $k \ge k_x$, the curve (17) intersects the k_x-axis at a finite distance,

$$k_x^* \sim k_0^{4/3}/k_{0x}^{1/3}. \tag{19}$$

We see that the zonostrophy cannot cascade too far to large k's, unless one starts with nearly zonal scales, $k_{0y} \gg k_{0x}$. In particular, if $k_{0y} = k_{0x}$ we have $k_x^* = 2^{1/6}k_0$, i.e. the maximal allowed wavenumber for the zonostrohy cascade is practically the same as the initial scale. In other words, in this case the zonostrophy can only cascade to the larger scales.
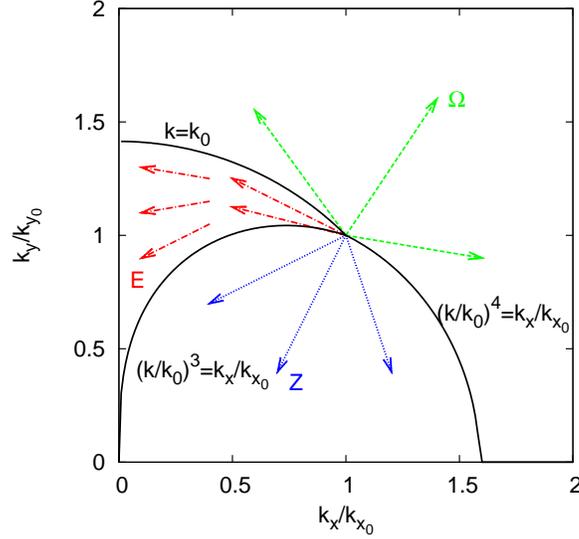
Fig. 2 Non-intersecting sectors for triple cascade as predicted by the generalized Fjørtoft argument.
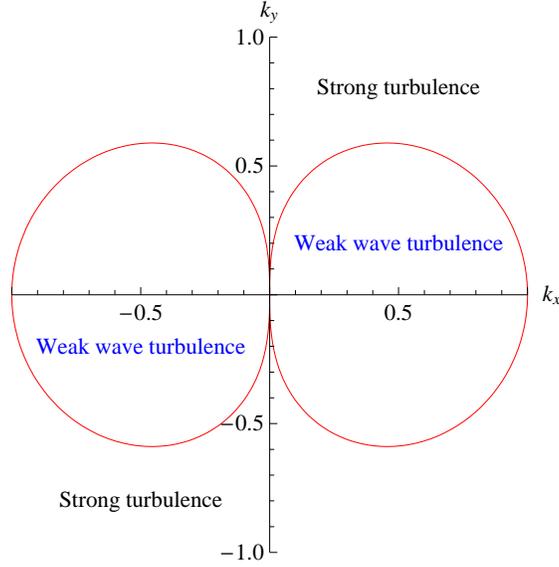
5.3 Alternative argument for zonation.

The generalized Fjørtoft argument presented above was based on the zonostrophy conservation which was proven for the wave kinetic equation and therefore, it is expected to work well for the weakly nonlinear case. However, later we are going to present numerics in which we "push" the formal boundaries of validity and test the performance of the triple cascade picture in the case when the initial nonlinearity is strong.

Because we are going to consider cases with strong nonlinearity, we would like to mention an alternative argument for zonation which makes sense when the initial turbulence is strong. Suppose that turbulence is forced strongly at large k's, so strongly that the linear term is negligible compared to the nonlinear one in the CHM equation (1). Since the linear term is the only source of anisotropy in the CHM model, the system is expected to build an isotropic inverse energy cascade identical to one of the 2D Navier-Stokes turbulence. As the inverse cascade progresses toward the larger scales, the linear dynamics (β-effect) become more and more important. A well-known boundary exists which defines the crossover from strong to weak turbulence, dominated by weakly nonlinear waves. This boundary is defined by the transitional wavenumber where the characteristic times of the linear and the nonlinear dynamics become equal. As it follows from the above speculation about the inverse cascade, the scaling for the nonlinear time has to be taken from a Kolmogorov-type estimate, $\tau_{NL} \sim (\varepsilon k^2)^{-1/3}$ and the linear time is just the inverse

wave frequency, $\tau_L = k^2/(\beta k_x)$. Equating τ_{NL} and τ_L we get

$$k^8 = k_\beta^5 k_x^3, \tag{20}$$

where $k_\beta = (\beta^3/\varepsilon)^{1/5}$. This curve is plotted in Fig. (3) and it is the well-known 'dumb-bell' or 'lazy 8' curve [32, 33]. For the modes which lie outside the curve, isotropic turbulence is the dominant process, whereas for those modes inside the dumb-bell, anisotropic Rossby wave turbulence is the dominant process.

Fig. 3 Dumb-bell curve in the Fourier space defining crossover from strong to weak turbulence.

The alternative zonation argument is based on the observation that weak wave turbulence is much less efficient in supporting the energy cascade than the strongly nonlinear interactions. Thus one can suppose that the energy cascade does not penetrate inside of the dumb-bell curve, but rather, it turns and continues along this curve to the larger scales. This condition that the linear and the nonlinear times are balanced *scale-by-scale* could be called a "critical balance", in analogy with similar arguments about the critical balance state discussed in MHD turbulence [34].

The critical balance picture would mean that the energy cascade path of zonation would be given by expression (20), which incidentally is very close to the path predicted by the Fjørtoft argument (17), if $k_0 \sim k_\beta$ (the power $3/8$ indeed very close to $1/3$).

A closer look reveals that the alternative zonation argument is actually not so "alternative" as it does not contradict our generalized Fjørtoft argument based on the zonostrophy concentration. Indeed, if the energy followed a path through the scales at which the linear and the nonlinear timescales balance then the zonostrophy

would flow below this path, i.e. to the weakly nonlinear scales. Thus, the zonos-
trophy would be supported at the weakly nonlinear scales and therefore would be
conserved (even though both the energy and the enstrophy would be supported in
the intermediately and strongly nonlinear scales in this case). But then all the three
invariants are conserved (no need for weak nonlinearity for conservation of E and
Ω) and the generalized Fjørtoft argument is once again valid.

One should also keep in mind that for the dumb-bell curve the estimation of the
shape is only approximate because it is based on the expression for τ_{NL} which is
valid, strictly speaking, only at k's which are much greater than the dumb-bell (i.e.
in the region of the isotropic inverse cascade). With this observation, we can put
together the "kinematic" view of the Fjørtoft argument and the "dynamic" critical
balance condition, and suggest that:

- Invariants E, Ω and Z cascade in the sectors prescribed by the generalized
  Fjørtoft argument, i.e. (16), (17) and (18).
- The energy cascade follows a path along the scales at which $\tau_{NL} \sim \tau_L$ which lies
  somewhere in the sector (17) and which does not strictly follow the dumb-bell
  prescription (20) (because of the unprecise definition of the dumb-bell discussed
  above).
- This picture is of course preceded by the usual isotropic inverse cascade of E in
  the case when the initial turbulence is very strong.

We emphasize that in this section we only considered the case when the initial
turbulence is strong. If the initial turbulence is weak, i.e. well within the dumb-bell,
then the energy cascade path remains in the weakly nonlinear scales (at least for a
while) rather than lie on the dumb-bell curve.

Now we will proceed to testing our theoretical predictions about the conservation
of the zonostrophy and the triple cascade behavior via numerical simulations of the
CHM equation in the Fourier space, Eqn (2).

6 NUMERICAL STUDY

A pseudospectral code has been written to solve equation (2). No dissipation is used
and the initial condition is given by

$$\hat{\psi}_{\mathbf{k}}|_{t=0} = A e^{\left(\frac{|\mathbf{k}-\mathbf{k_0}|^2}{k_*^2} + i\phi_{\mathbf{k}} \right)} + \text{image}, \tag{21}$$

where k_0 and k_* are constants and $\phi_{\mathbf{k}}$ are random independent phases, and by "im-
age" we mean the mirror-reflected spectrum with respect to the k_x axis. Note that
only the semi-plane $k_x \geq 0$ was used in our computations because of the symmetry
$\hat{\psi}_{-\mathbf{k}} = \hat{\psi}_{\mathbf{k}}^*$ arising from the fact that the streamfunction ψ in the CHM equation (1)
is a real function.

We opted to simulate such an evolving non-dissipative system rather than a
forced/dissipated steady-state turbulence considered by the Fjørtoft argument be-

cause it appears to be more physically relevant (since there appears to be no physically meaningful dissipation acting selectively on nearly zonal and nearly meridional scales only). Yet, we hope that the cascade picture obtained via the Fjørtoft argument is meaningful for such decaying turbulence too, similar to what appears to be the case e.g. in the 2D Navier-Stokes turbulence.

Of course, when calculating a non-dissipative system one has to be aware of the possible bottleneck accumulation of turbulence near the maximum wavenumber after the turbulent front reaches these scales. Thus we make sure to stop our simulations before this happens.

6.1 Centroids

To quantify the cascades of the energy, enstrophy and zonostrophy in the time-evolving non-dissipative turbulence we introduce the *centroids* ("centres of mass") of the total of each invariant defined respectively as follows,

$$\mathbf{k}_E(t) = \frac{1}{E} \int \mathbf{k}\, k^2 |\hat{\psi}_k|^2 \, d\mathbf{k}, \tag{22}$$

$$\mathbf{k}_\Omega(t) = \frac{1}{\Omega} \int \mathbf{k}\, k^4 |\hat{\psi}_k|^2 \, d\mathbf{k}, \tag{23}$$

$$\mathbf{k}_Z(t) = \frac{1}{Z} \int \mathbf{k}\, \frac{k_x^4}{k^6} (k_x^2 + 5k_y^2) |\hat{\psi}_k|^2 \, d\mathbf{k}. \tag{24}$$

Of course, it is not *apriori* clear if the Fjørtoft argument formulated for the steady-state forced/dissipated turbulence has a predictive power for the trajectories of the centroids in the *k*-space. In the present paper we "experimentally" verify that this is indeed the case.

For the 2D Navier-Stokes (Euler), it is actually possible to recast the Fjørtoft argument for the non-dissipative evolving turbulence directly in terms of the centroids in a rigorous way, see Appendix B. However, the structure of the CHM is more involved and it is not clear if one can produce a generalized Fjørtoft's argument for the triple cascades in terms of the centroids in a rigorous way. This is certainly an interesting question to be addressed in future. [1]

---

[1] We have been able to find some of the relevant inequalities in terms of the centroids, but most of the conditions restricting the triple cascade sectors are still missing.

6.2 Settings for the weakly nonlinear and the strongly nonlinear runs.

We have chosen two sets of parameters to be used in two runs corresponding to weak and strong initial nonlinearities respectively.

The weakly nonlinear and the strongly nonlinear runs were performed at resolutions 512^2 and 1024^2 respectively. This is because the weakly nonlinear systems evolve much slower that the strongly nonlinear ones and one has to compute them for much longer. Correspondingly, the centre of the initial spectrum and its width were chosen to be $\mathbf{k_0} = (20, 20)$ and $k_* = 8$ in the weakly nonlinear run and $\mathbf{k_0} = (40, 40)$ and $k_* = 16$ in the strongly nonlinear run.

The initial amplitudes in the weakly nonlinear and the strongly nonlinear runs are $A = 10^{-6}$ and $A = 5 \times 10^{-7}$ respectively. Determining the relevant degree of nonlinearity σ that corresponds to these initial conditions is tricky. One can directly estimate the linear and the nonlinear terms in the Eqn (2) and take into account the fact that there will be statistical cancellations in the sum of the nonlinear term due to the random phases, i.e. schematically

$$\left| \sum_{j=1}^{N} \text{individual-term}_j \right| \sim \sqrt{N} \, |\text{individual-term}| .$$

This way we get an estimate

$$\sigma \sim \frac{2\sqrt{2\pi}k_0^3 k_* A}{\beta}, \tag{25}$$

which gives $\sigma \sim 0.09$ for the weakly nonlinear run and $\sigma \sim 0.7$ for the strongly nonlinear run. However, it is likely that in the strongly nonlinear case the phases will quickly become correlated to a certain degree. Evaluating the nonlinear term in the extreme case when the phases are totally coherent would give an extra factor of $\sqrt{N} \sim 2\sqrt{\pi k_*^2} \sim 100$, so we would have for the strongly nonlinear run $\sigma \sim 70$, which obviously is an overestimate. From common sense, in a non-rigorous way, we believe that the true relevant value for σ in this case is closer to the random-phase estimate, but perhaps slightly higher, e.g. $\sigma \sim 1 - 2$, which is approximately "on the dumb-bell".

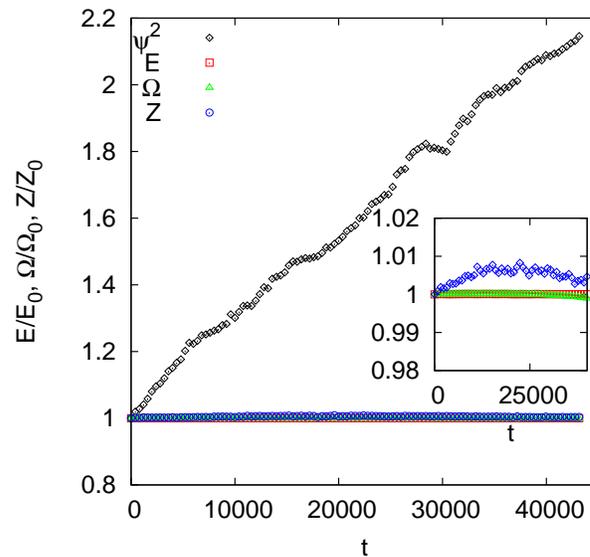## 6.3 Weakly Nonlinear Case

For this case, the degree of nonlinearity is weak, $\sigma \sim 0.09$, so that the initial turbulence is well within the dumb-bell. Fig. (4) shows the conservation of each invariant. Because of the slow weakly nonlinear evolution, any quantity proportional to the turbulent intensity could look "conserved", so to demonstrate the true conservation of the zonostrophy we plot its time evolution along with a non-conserved

quantity, $\int \psi^2 \, d\mathbf{x}$. It is clear that all three invariants, E, Ω and Z are well conserved. Namely, the energy is conserved within 0.01%, the enstrophy - within 0.15% and the zonostrophy is conserved within 1 %. Note that this is a first numerical demonstration of the conservation of the zonostrophy invariant. We remind the reader that Z is precisely conserved by the wave kinetic equation (9) and therefore its conservation by the dynamical CHM equation (2) is subject to the applicability conditions of this kinetic equation, namely the weak nonlinearity and the random phases. It is not *apriori* clear how well these conditions are satisfied throughout the k-space (particularly near the zonal scales).

The cascade directions for E, Ω and Z are plotted in Fig. (5) in terms of the paths followed by the respective centroids, (22), (23) and (24). Note that for convenience we normalize the centroids to their initial values, $k_{E0}^c, k_{\Omega 0}^c$ and k_{Z0}^c (which are different from k_0) so that the centroid paths start from the same point in Fig. (5).

In Fig. (5) we see that each invariant cascades well into its predicted sector. Interestingly, the enstrophy and the zonostrophy paths are well inside their respective cascade sectors, whereas the energy follows the boundary of its sector with the zonostrophy sector. One should remember, however, that the boundaries between the sectors are not sharp because the Fjørtoft argument operates with strong inequalities ($\ll$ and $\gg$ rather than $<$ and $>$).

Fig. 4 Conservation of energy, enstrophy and zonostrophy for the weakly nonlinear case. Non-conserved quantity Ψ^2 also shown.

Three successive frames of the energy spectrum in the 2D k-space along with the x-space frames of vorticity distributions at the same moments of time for the weak nonlinearity case are shown in Fig. (8). The initial spectrum, which represents a
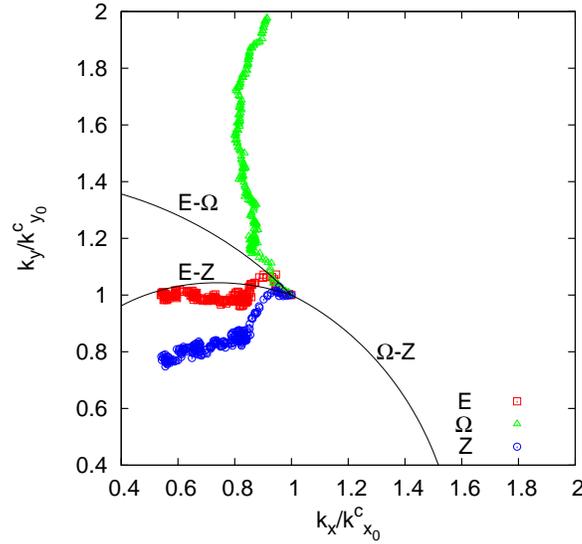
Fig. 5 The cascades of energy, enstrophy and zonostrophy for the weakly nonlinear case, tracked by their centroids.

gaussian spot centered at $\mathbf{k_0}$ and its mirror image, is seen to grow "arms" toward the coordinate origin, so that a closed "ring" forms and then starts shrinking in size. The ring is suggestive of the dumb-bell shape (when complemented with the other half of the distribution at $k_x < 0$), although the similarity is only visual rather than quantitative, because the nonlinearity is quite small. Presumably, the growing of arms and the ring shrinking are indicative of the structure of the anisotropic inverse energy cascade process. On the respective vorticity x-plots, we see initial dominant short-wave components propagating at $\pm 45^o$ (corresponding to the position of the initial maxima in the spectrum) which in time evolve into a more disordered turbulent state with a predominant zonal orientation.
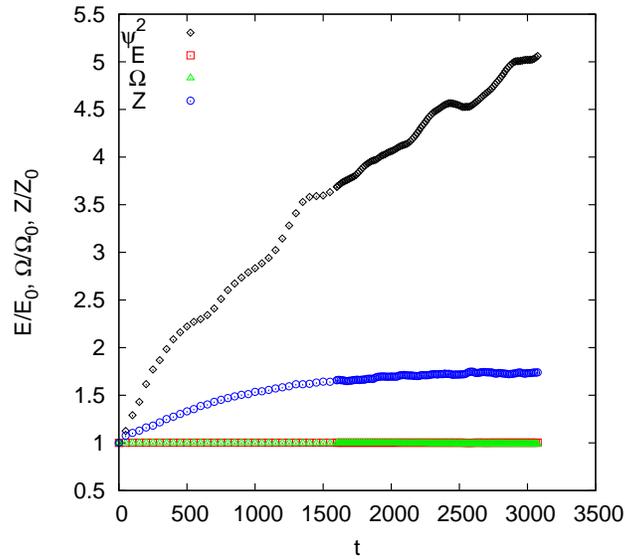
6.4 Strongly Nonlinear case

For this case, $\sigma \sim 1 - 2$ so that the initial turbulence is near the boundary of the dumb-bell. Fig. (6) shows the conservation of each invariant. While the energy and enstrophy are still well conserved (the energy within 0.2% and the enstrophy - within 1.2%), the zonostrophy is not conserved initially. This is not surprising considering that the zonostrophy is only expected to be conserved if the nonlinearity is weak. What is more interesting, however, is that the zonostrophy growth saturates as time proceeds, so that the zonostrophy is rather well conserved in this case for large times. This suggests, as we argued before, that for large times the scales that support the

zonostrophy invariant are weakly nonlinear, even though the energy scales proba-
bly remain moderately nonlinear, and the enstrophy scales are definitely strongly
nonlinear.

The cascade paths for E, Ω and Z in terms of the respective centroids are plotted
in Fig. (7). Once again we see a picture which is similar to the one already observed
for the weakly nonlinear case: the enstrophy and the zonostrophy cascades lie well
inside their respective theoretically predicted sectors, and the energy cascade fol-
lows the boundary of its sector. It is quite possible that the energy path lies in the
"critically balanced" scales where the nonlinear and the linear time scales are of
the same order. However the measurement of the nonlinear time scale is quite am-
biguous and it is still unclear if the critical balance approach can be formulated in
a more precise way in this case. In any case, one can clearly see that even in this
strongly nonlinear case the zonostrophy invariant is conserved for large times, and
that the triple cascade picture predicted using this invariant provides a reasonable
description of the turbulence evolution and explanation of the zonal jet formation.

We have also looked at the energy spectra in the 2D wavenumber space and at the
2D vorticity distributions on the x-plane evolving in time, see Fig. (9). The essential
features of the evolution of these distributions appeared to be remarkably similar
to the ones of the weakly nonlinear case, with somewhat more evident zonal jets
at later times. This can be explained by the fact that the strongly nonlinear systems
evolve faster than the weakly nonlinear ones, so that what we see here is a more
advanced stage of zonation.

Fig. 6 Conservation of energy, enstrophy and zonostrophy for the strongly nonlinear case. Non-
conserved quantity Ψ^2 also shown.
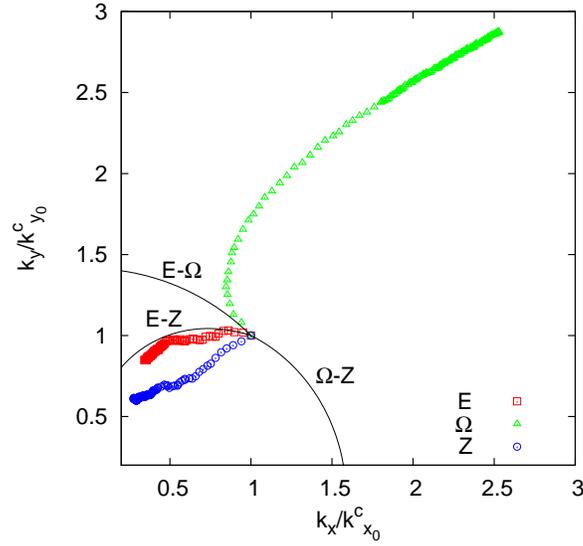
Fig. 7 The cascades of energy, enstrophy and zonostrophy for the strongly nonlinear case, tracked by their centroids.

7 SUMMARY

In the present paper the generalized Fjørtoft argument was used to predict a triple cascade behaviour of the CHM turbulence, in which the energy, the enstrophy and the zonostrophy are cascading into their respective non-intersecting sectors in the scale space. These cascades are anisotropic and the energy cascade is predicted to be directed to the zonal scales, which provides a physical explanation and the character of the formation of the zonal jets in such systems.

The zonostrophy conservation, as well as the triple cascade picture, were tested numerically for the cases of both weak and strong initial nonlinearities. The zonostrophy invariant was shown to be well conserved in the weakly nonlinear case. Moreover, the zonostrophy conservation was also observed for the case with strong initial nonlinearity after a transient non-conservative time interval. Presumably, this is because the zonostrophy moves in time to the scales that are weakly nonlinear (even though the energy and the enstrophy remain in the strongly nonlinear parts of the Fourier space). Using the energy, the enstrophy and the zonostrophy centroids for tracking the transfers of these invariants in the Fourier space, we demonstrated that all the three invariants cascade as prescribed by the triple cascade Fjørtoft argument in both the weakly nonlinear and in the strongly nonlinear cases. The energy appears to be somewhat special among the three invariants in that it tends to cas-
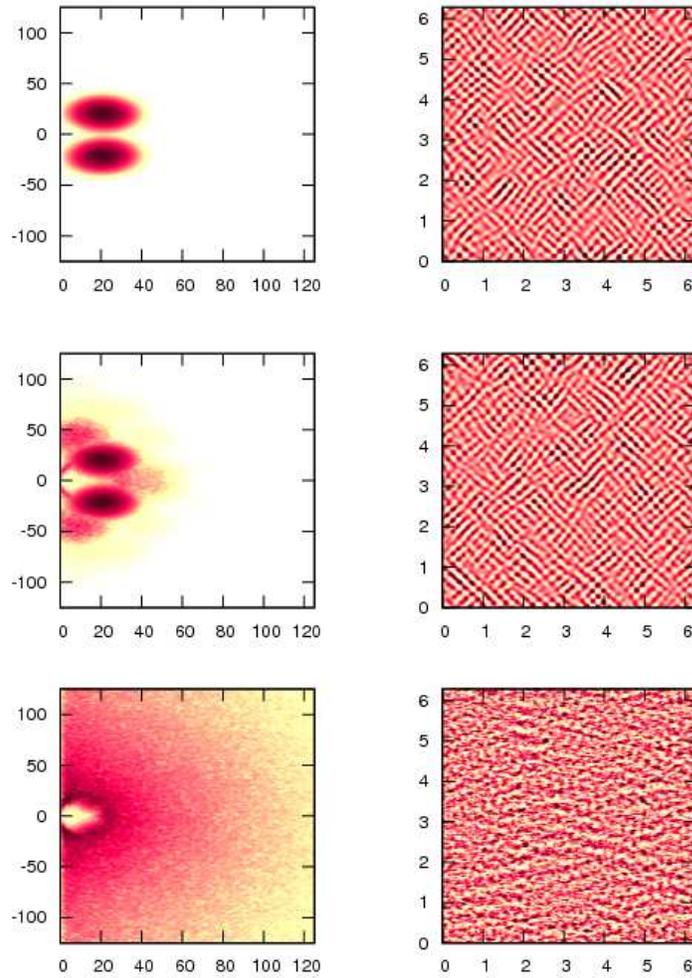
Fig. 8 Contour plots of the 2*D* energy spectrum in *k*-space (left) and corresponding contours of vorticity in *x*-space (right) for the weakly nonlinear case.
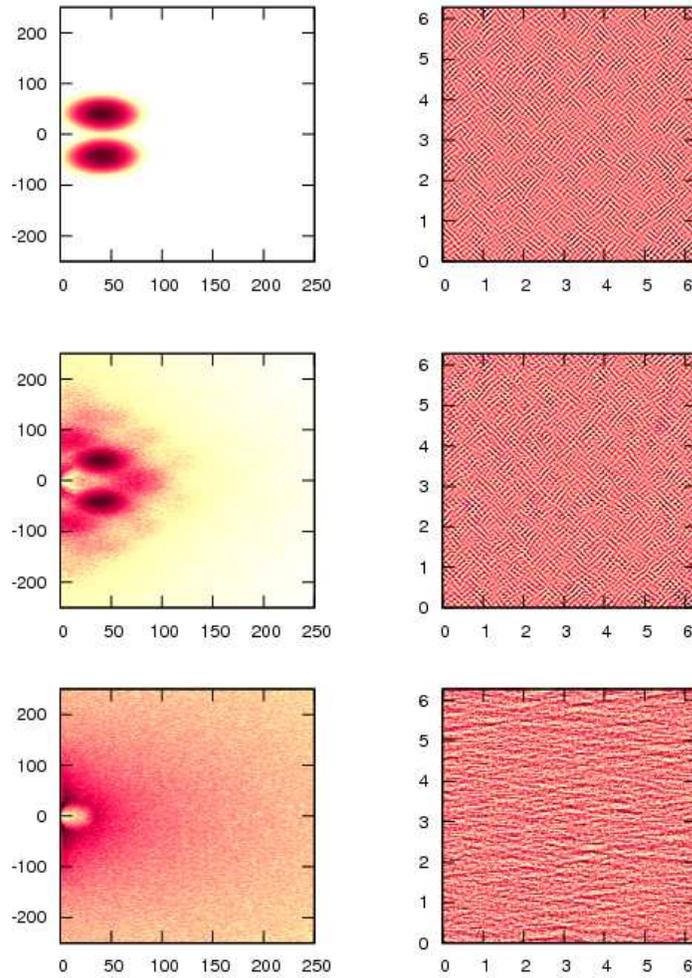
Fig. 9 Contour plots of the 2*D* energy spectrum in *k*-space (left) and corresponding contours of vorticity in *x*-space (right) for the strongly nonlinear case.

cade along the edge of the sector allowed by the Fjørtoft argument, namely along the curve $k \propto k_x^{1/3}$.

We believe that further studies would be helpful, both theoretical and numerical, for establishing the conditions under which the zonostrophy is conserved, in particular finding out the extent to which the statistical properties of the system (e.g. random phases) are important in addition to weak nonlinearity of the zonostrophy supporting scales. It would be also interesting to study the behaviour of zonostrophy in the other setups within the CHM model, e.g. the modulational instability and truncated systems of coupled resonant triads.

References

1. Balk, A.M., Nazarenko, S.V. and Zakharov, V.E.: On the structure of the Rossby/drift turbulence and zonal flows. Proceedings of the International Symposium "Generation of Large-Scale Structures in Continuous Media", Perm-Moscow, USSR, 34–35 (1990).
2. Balk, A.M., Nazarenko, S.V. and Zakharov, V.: New Invariant for Drift Turbulence. Physics Letters A **152**, 276–280 (1991)
3. Gill, A.E.: Atmosphere - Ocean Dynamics. Academic Press, New York (1982)
4. Simon, A. A.: The structure and temporal stability of Jupiter's zonal winds: A study of the north tropical region. Icarus **141**, 29 (1999).
5. Sanchez-Lavega, A., Rojas, J. F. and Sada, P. V.: Saturn's zonal winds at cloud level. Icarus **47**, 405 (2000).
6. Galperin, B., Nakano, H., Huang ,H.-P. and Sukoriansky, S.: The ubiquitous zonal jets in the atmospheres of giant planets and Earth's oceans. Geophys. Res. Lett. **131**, (2004) L13303, doi:10.1029/2004GL019691.
7. Maximenko N.A., Melnichenko, O.V., Niiler, P.P. and Sasaki, H.: Stationary mesoscale jet-like features in the ocean. Geophys. Res. Lett. **135**, (2008) L08603, doi:10.1029/2008GL033267.
8. Gill, A.E.: The stability on planetary waves on an infinite beta-plane. Geophys. Fluid Dyn. **6**, 29-47 (1974).
9. Manin, D.Y. and Nazarenko, S.V.: Nonlinear interaction of small-scale Rossby waves with an intense large-scale zonal flow. Phys. Fluids. A **6**, 1158-1167 (1994).
10. Lewis, J.M.: Clarifying the Dynamics of the General Circulation: Phillips's 1956 Experiment. Bulletin of the American Meterological Society **79 No. 1**, (1988).
11. James, I.N.: Suppression of Baroclinic Instability in Horizontally Sheared Flows. J.Atmo.Sci., **44 No. 24**, 3710 (1987).
12. Balk, A.M., Nazarenko, S.V. and Zakharov, V.E.: On the Nonlocal Turbulence of Drift Type Waves. Phys.Lett.A **146**, 217–221 (1990);
13. Balk, A.M., Nazarenko, S.V. and Zakharov, V.E.: Nonlocal Drift Wave Turbulence. Sov.Phys.-JETP **71**, 249–260 (1990).
14. Wagner, F. et al.: Phys. Rev. Lett. **49**, 1408 (1982).
15. Diamond, P. H., Itoh, S.-I., Itoh, K. and Hahm, T. S.: Zonal flows in plasma - a review. Plasma Phys. Control. Fusion **47 No.5** R35–R161(2005).
16. Lorentz, E.N.: Barotropic instability of Rossby wave motion. J.Atmo.Sci. **29**, 258–269 (1972).

17. Mima, K. and Lee, Y. C.: Modulational instability of strongly dispersive drift waves and formation of convective cells. Physics of Fluids **23**, 105 (1980).
18. Smolyakov, A.I., Diamond, P.H. and Shevchenko, V.I.: Phys. Plasmas **7**, 1349 (2000).
19. Onishchenko O.G., Pokhotelov O.A., Sagdeev R.Z. et al.: Nonlin. Processes Geophys. **11**, 241 (2004).
20. Smolyakov, A.I. and Krasheninnikov, S. I.: Phys. Plasmas **15**, 072302 (2008)
21. Connaughton, C., Nadiga, B., Nazarenko, S. and Quinn, B.: Modulational instability of Rossby and drift waves and generation of zonal jets, *in preparation.*
22. Williams, G. P.: Planetary circulations : Barotropic representation of Jovian and terrestrial turbulence. J. Atmos. Sci. **35**, 1399–426 (1978)
23. Rhines, P.B.: Geostrophic Turbulence. Ann. Rev. Fluid Mech. **11**, 401–441 (1979).
24. Fjørtoft, R.: On the changes in the spectral distribution of kinetic energy for two-dimensional non-divergent flow. Tellus **5**, 225–230 (1953).
25. Kraichnan, R.H.: Phys. Fluids **10**, 1417 (1967).
26. Rhines, P.: Waves and turbulence on a betaplane. J. Fluid Mech. **69**, 417–443 (1975).
27. Balk, A.M.: A New Invariant for Rossby Wave Systems. Physics Letters A **155**, 20–24 (1991).
28. Balk, A.M.: SIAM Review, **39 No. 1**, 68–94 (1997).
29. Balk, A.M.: Angular distribution of Rossby wave energy. Physics Letters A **345**, 154–160 (2005).
30. Charney, J. G.: On a physical basis for numerical prediction of large-scale motions in the atmosphere. J. Meteor. **6**, 371–85 (1949).
31. Hasegawa, A. and Mima, K.: Pseudo-Three-Dimensional Turbulence in Magnetised Nonuniform Plasma. Phys. Fluids **21 1**, 87–92 (1978).
32. Holloway, G.: Contrary roles of Planetary Wave Propagation in Atmospheric Predictability, in: Predictability of Fluid Motions edited by: Holloway, G. and West, B., 593–599, American Institute of Physics, New York, (1984).
33. Vallis, G. and Maltrud, M.: Generation of Mean flows and Jets on a β-Plane and over Topography. J.Phys. Oceanography **23**, 1346–1362 (1993).
34. Goldreich, P. and Sridhar, S.:Toward a theory of interstellar turbulence. 2: Strong Alfvénic turbulence. Astrophysical Journal, Part 1 (ISSN 0004-637X), **438 no. 2**, 763–775 (1995).

Appendix A - Small-scale limit of Zonostrophy

The general expression for the zonostrophy density is given by [27]:

$$\zeta = \arctan\frac{k_y - k_x\sqrt{3}}{\rho k^2} - \arctan\frac{k_y + k_x\sqrt{3}}{\rho k^2}$$ (26)

Expanding this expression in the powers of $1/\rho$ up to ninth order, we get

$$\begin{aligned}\zeta =\ & -2\sqrt{3}\frac{k_x}{\rho k^2} + 2\sqrt{3}\frac{k_x}{\rho^3 k^4} \\ & -2\sqrt{3}\frac{k_x}{\rho^5 k^{10}}[k_y^4 + 6k_x^2 k_y^2 + \frac{9}{5}k_x^4] \\ & +2\sqrt{3}\frac{k_x}{\rho^7 k^{14}}[\frac{27}{7}k_x^6 + 27k_x^4 k_y^2 + 15k_x^2 k_y^4 + k_y^6] \\ & -2\sqrt{3}\frac{k_x}{\rho^9 k^{18}}[9k_x^8 + 108k_x^6 k_y^2 + 126k_x^4 k_y^4 \\ & +28k_x^2 k_y^6 + k_y^8] + O(\rho^{-10}).\end{aligned}$$

We note that the Taylor expansion of the frequency $\omega_k = -\beta/(k^2 + \rho^{-2})$ in the powers of $1/\rho$ is

$$\omega_k = \sum_{n=1}^{\infty} \omega^{(n)} = \sum_{n=1}^{\infty} \frac{(-1)^n \beta \rho^2 k_x}{(\rho k)^{2n}}. \tag{27}$$

We see that in the leading order $\zeta = \frac{2\sqrt{3}}{\beta\rho}\omega_k$, i.e. in the small-scale limit ζ is proportional to the energy and not an independent invariant.

Thus, to find the truly independent invariant in the small-scale limit we must subtract this "energy" part. To have a simpler expression which is ρ-independent in the leading order, we will also multiply the result by $-\frac{5\rho^5}{8\sqrt{3}}$. Re-defined this way, the zonostrophy invariant is

$$\tilde{\zeta} = -\frac{5\rho^5}{8\sqrt{3}}(\zeta - 2\sqrt{3}\omega/\beta\rho) =$$

$$k_x^3 \left(\frac{5k_y^2 + k_x^2}{k^{10}} - 5\frac{\frac{5}{7}k_x^4 + 6k_x^2 k_y^2 + 3k_y^4}{\rho^2 k^{14}} + 5\frac{2k_x^8 + 26k_x^6 k_y^2 + 30k_x^4 k_y^4 + 6k_x^2 k_y^2}{\rho^4 k^{18}} \right),$$

which in the limit $\rho \to \infty$ becomes the expression we were looking for,

$$\tilde{\zeta} = k_x^3 \frac{k_x^2 + 5k_y^2}{k^{10}}. \tag{28}$$

Appendix B - Fjørtoft argument in terms of the centroids.

Let us consider an evolving hydrodynamic 2D turbulence in the absence of forcing and dissipation. Here we will re-formulate the Fjørtoft argument in terms of the energy and enstrophy centroids in the k and l (i.e. scale) spaces. This formulation will be rigorous and quite useful for visualizing the directions of transfer of of the energy and the enstrophy. In contrast with the version of the Fjørtoft argument give in the main text, this formulation is for a non-dissipative turbulence rather than a forced/dissipated system.

The energy and the enstrophy k-centroids are defined respectively as

$$k_E = \int_0^{\infty} k E_k \, dk / E, \tag{29}$$

$$k_{\Omega} = \int_0^{\infty} k^3 E_k \, dk / \Omega, \tag{30}$$

and the energy and the enstrophy l-centroids as defined respectively as

$$l_E = \int_0^{\infty} k^{-1} E_k \, dk / E, \tag{31}$$

$$l_{\Omega} = \int_0^{\infty} k E_k \, dk / \Omega \equiv k_E E / \Omega, \tag{32}$$

where E_k is the 1D energy spectrum (i.e. the energy density in $|k|$).

Theorem 1. *Assuming that the integrals defining $E, \Omega, k_E, k_\Omega, l_E$ and l_Ω converge, the following inequalities hold,*

$$k_E \leq \sqrt{\Omega/E}, \tag{33}$$

$$k_\Omega \geq \sqrt{\Omega/E}, \tag{34}$$

$$k_E k_\Omega \geq \Omega/E, \tag{35}$$

$$l_E \geq \sqrt{E/\Omega}, \tag{36}$$

$$l_\Omega \leq \sqrt{E/\Omega}, \tag{37}$$

$$l_E l_\Omega \geq E/\Omega. \tag{38}$$

We are going to prove this theorem using Cauchy-Schwartz inequality [2], which states that

$$\left| \int_0^\infty f(k)g(k)\, dk \right| \leq \left| \int_0^\infty f^2(k)\, dk \right|^{1/2} \left| \int_0^\infty g^2(k)\, dk \right|^{1/2}$$

for any functions $f(k), g(k) \in L^2$. We will only deal with positive functions, so the absolute value brackets may be omitted. Being in L^2 in our case means that all the relevant integrals converge, as suggested in the statement of the problem.

First, let us consider integral $\int kE\, dk$ and apply Cauchy-Schwartz inequality as follows,

$$\int_0^\infty kE\, dk = \int_0^\infty (kE^{1/2})(E^{1/2})\, dk \leq \left(\int_0^\infty k^2 E\, dk \right)^{1/2} \left(\int_0^\infty E\, dk \right)^{1/2},$$

which immediately yields (33) and (37).

Second, let us consider $\Omega = \int k^2 E\, dk$ and split it as,

$$\int_0^\infty k^2 E\, dk = \int_0^\infty (k^{3/2}E^{1/2})(k^{1/2}E^{1/2})\, dk \leq \left(\int_0^\infty k^3 E\, dk \right)^{1/2} \left(\int_0^\infty kE\, dk \right)^{1/2},$$

which immediately yields (35). Combining (35) with (33) gives (34).

Now, let us split $\int kE\, dk$ in a different way,

$$\int_0^\infty kE\, dk = \int_0^\infty (k^{3/2}E^{1/2})(k^{-1/2}E^{1/2})\, dk \leq \left(\int_0^\infty k^3 E\, dk \right)^{1/2} \left(\int_0^\infty k^{-1} E\, dk \right)^{1/2},$$

which immediately yields (38). Combining (38) with (37) gives (36).

We see that according to inequalities (33) and (34), during the system's evolution the energy centroid $k_E(t)$ is bounded from above and the enstrophy centroid $k_\Omega(t)$

---

[2] The suggestion to use the Cauchy-Schwartz inequality for reformulating the Fjørtoft argument in terms of the centroids was made to us by Gregory Eyink during the INI workshop the proceedings of which are published in this book.

is bounded from below (both by the same wavenumber $k = \sqrt{\Omega/E}$), as one would expect from Fjørtoft argument. Further, inequality (35) means that if $k_E(t)$ happened to move to small k's then $k_\Omega(t)$ *must* move to large k's, that is roughly, there cannot be inverse cascade of energy without a forward cascade of enstrophy. Note that there is no complimentary restriction which would oblige $k_E(t)$ to become small when $k_\Omega(t)$ goes large, so the k-centriod part of the Fjørtoft argument is asymmetric, and one has to consider the l-centroids to make it symmetric. Indeed, in additions to conditions (36) and (37) which are similar to (33) and (34), we have inequality (38) meaning that if $l_\Omega(t)$ happened to move to small l's then $l_E(t)$ *must* move to large l's, i.e. any forward cascade of enstrophy must be accompanied by an inverse cascade of energy.

Importantly, we do not always have $k_E \sim 1/l_E$ and $k_\Omega \sim 1/l_\Omega$. Indeed, consider a state with spectrum $E_k \sim k^{-5/3}$ for $k_a < k < k_b$ (with $k_b \gg k_a$) and $E_k \equiv 0$ outside of this range. It is easy to see that for this state $k_E \sim k_b^{1/3} k_a^{2/3}$ and $l_E \sim 1/k_b$ (i.e. $k_E \nsim 1/l_E$) and $k_\Omega \sim 1/l_\Omega \sim k_b$.